PAPER • OPEN ACCESS

Balanced torsionally oscillating pipe used as a viscosity sensor

To cite this article: S Clara *et al* 2019 *Meas. Sci. Technol.* **30** 015101

View the article online for updates and enhancements.

Balanced torsionally oscillating pipe used as a viscosity sensor

S Clara[1] , **F Feichtinger**[1], **T Voglhuber-Brunnmaier**[1,2], **A O Niedermayer**[1], **A Tröls**[1] **and B Jakoby**[1]

[1] Institute for Microelectronics and Microsensors, Johannes Kepler University Linz, Linz, Austria
[2] Linz Institute of Technology, Johannes Kepler University Linz, Linz, Austria

E-mail: Stefan.Clara@jku.at

CrossMark

Abstract

We present a robust viscosity measurement system based on a torsionally oscillating pipe. The sensitive surface of the sensor performs periodic movements in the fluid to be sensed, generating a shear wave that penetrates the fluid. Due to this interaction, the resonance characteristic of the structure is affected, in particular the quality factor decreases with increasing viscosity. The pipe is mounted at its center where it features a nodal point of the preferred resonant mode, reducing temperature issues while simultaneously enabling high quality factors. A mathematical model is presented illustrating how different parameters influence the sensitivity of the sensor. Long-term measurements were performed to demonstrate the time stability of the sensor setup.

Keywords: viscosity, resonant, flow-through, sensor

(Some figures may appear in colour only in the online journal)

Introduction

In chemical or biochemical industrial applications, a huge number of sensors is utilized to monitor production processes [1]. The obtained data is used to actively control the evolution of the reactions in order to, for example, maintain the quality of the synthesized products or keep the amount of waste as low as possible [2]. In such systems, physical fluid property sensors are used to determine characteristics such as density or viscosity. To this end, several measurement devices are already on the market [3, 4]. Various sensor designs have been presented over the years [5–7]. For sensing viscosity, resonant sensor systems offer particularly high sensitivity. Many different designs have been presented, such as in [8–11] or [12], in which most operate in the higher-frequency regime above 20 kHz or in the MHz regime. Sometimes these sensors are small and fragile and thus not suited for use in production plants. The high resonance frequency results in a very thin fluid layer being sensed directly on the surface of the sensor

[13]. The adhesion of particles at the sensor surface can cause major problems.

The sensor setup presented in this work was designed to work in the low-frequency regime below 10 kHz, where the penetration depth of the imposed shear displacement is increased avoiding the aforementioned problems. We introduced the concept for this setup only recently [14]. In this paper, we present the design process of the sensor. In addition, a more accurate mathematical model taking the fluid damping into account is introduced. Long-term measurements are performed for different temperatures and finally the accuracy of the sensor system is reviewed.

Setup

The demonstrator device is machined of aluminium. Figure 1 shows a cross-section of the sensor setup. The sensor is based on two coaxially aligned pipes where the outer one, featuring two flywheels with permanent magnets, is actuated to perform torsional oscillations by means of magnetic fields. The sensitive part of the device is the outer pipe shown in figure 1(3) ($d_o = 12$ mm, $d_i = 8$ mm, $l = 130$ mm). Two flywheels
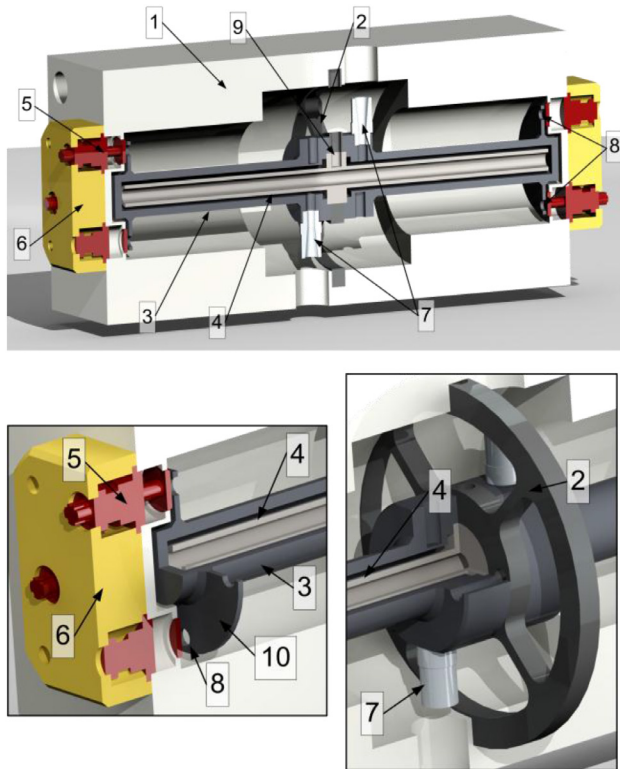
Figure 1. Cross-section of the sensor setup consisting of (1) housing, (2) mounting spring, (3) oscillating outer pipe, (4) inner pipe, (5) electromagnetic actuation coil, (6) coil housing, (7) in/outlet with Luer lock adapter, (8) holes for permanent magnets, (9) hole for a temperature sensor, and (10) flywheel.

are located at the ends of this pipe ($d = 30$ mm, $h = 1$ mm figure 1(10)), each containing four neodymium permanent magnets ($d = 3$ mm, $h = 1$ mm, figure 1(8)) that are used for the actuation and readout of the oscillations. The inner pipe ($d_o = 6$ mm, $d_i = 4$ mm, $l = 64$ mm, figure 1(4)) is coaxially aligned to the outer pipe. This pipe does not move during the measurements and is only used to guide the fluid through the sensor to achieve a homogeneous filling of the measurement chamber. The center of the pipe structure is attached to a mechanical spring ($d = 60$ mm, $h = 4$ mm, figure 1(2)) whose other end is mounted to the surrounding housing ($140 \times 70 \times 70$ mm³, figure 1(1)) and is used to mechanically decouple the pipes from the housing. The center of the pipe structure is also the nodal point of the torsional oscillation mode. If the outer pipe oscillates in this mode, the nodal point does not move and little energy is coupled into the housing or into the inner pipe. On each side of the sensor housing, four electromagnetic coils (figure 1(5)) are placed. These coils are rotated by 10° with respect to the equilibrium position of the permanent magnets mounted into the flywheels (figure 1(8)). Due to this angular displacement, a rotatory force acts on the flywheels once the coils are driven accordingly. The coils are protected by the coil housing figure 1(6). For the filling of the sensor with fluid, two Luer lock adapters (figure 1(7)) are screwed to the outer pipes. For temperature measurements, a hole is drilled in the mounting spring and the inner pipe, where a temperature sensor such as a PT100 can be placed (figure 1(9)).

In the demonstrator setup, the two Luer lock connectors (figure 1(7)) are placed on the flange of the outer pipe as close as possible to the mounting spring. The fluid is filled from the inlet (figure 1(7)), from where it flows into the cylindrical space between the inner and outer pipe to the left end of the sensor, through the inner pipe on the right side of the sensor, then from the right side into the cylindrical space between the inner and outer pipe to the outlet, which is located opposite to the inlet. Due to this special pipe system, the sensor can be used as a flow-through sensor.

The sensor setup offers different oscillation modes which can be used to determine the viscosity and/or density of a liquid. All these modes have different characteristics and yield different sensitivities. The lowest order modes are illustrated in figure 4. The most interesting mode for viscosity measurements is the anti-symmetric (torsional) mode. In this mode the outer pipe itself acts as a torsional spring and the two flywheels on the end oscillate against each other, i.e. inversely phased. The center of the pipe's axis is the nodal point of this torsional oscillation mode, which means that ideally the points located at the circumference of the pipe are not moving. As the resonator structure is attached to the mounting spring at this point, little energy is transferred to the housing of the sensor. This enables very high quality factors and thus higher sensitivities particularly for low viscous fluids. The inner surface of the outer pipe interacts with the fluid. As the surface velocities vary along the longitudinal axis of the pipe according to the mode shape, the sensitivity of the sensor is higher at the ends of the pipe.

Actuation and readout

For the actuation and readout, electromagnetic coils are used. Combined with the permanent magnets in the flywheels, they are used to excite different mechanical oscillation modes. The most interesting mode for viscosity measurements is the torsional mode (see figure 4). For the demonstrator setup we used two coils on each side of the sensor. The coils on the left side were used to actuate the resonator and the coils on the right side were used as readout coils. It is also possible to implement the actuation and the readout on the same side of the sensor but in this case the cross-talk between the coils has to be eliminated by arranging the permanent magnets and choosing the winding direction of the coils accordingly. For the implemented separated actuation and readout, the cross-talk is not a problem due to the distance between both ends of the pipe. The force acting on the permanent magnets is linearly related to the current through the actuation coils. (Note: Due to the one-sided actuation principle, a spurious force along the axial direction of the pipe also acts on the sensor. This force could be compensated by using the abovementioned symmetric arrangement of actuation coils at both ends of the sensor pipe.) The readout signal is generated due to the movement of the permanent magnets in the vicinity of the coils. The induced voltage depends on the rate of change of the magnetic flux density in the coils. Therefore, the induced voltage is related to the velocity of the permanent magnets. As
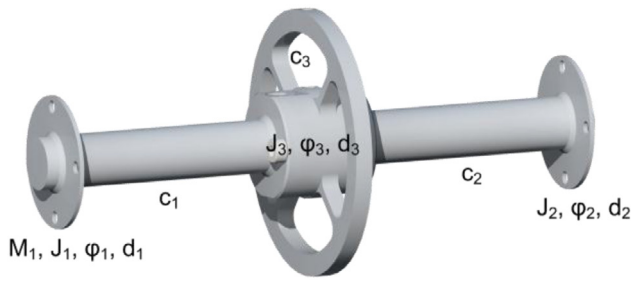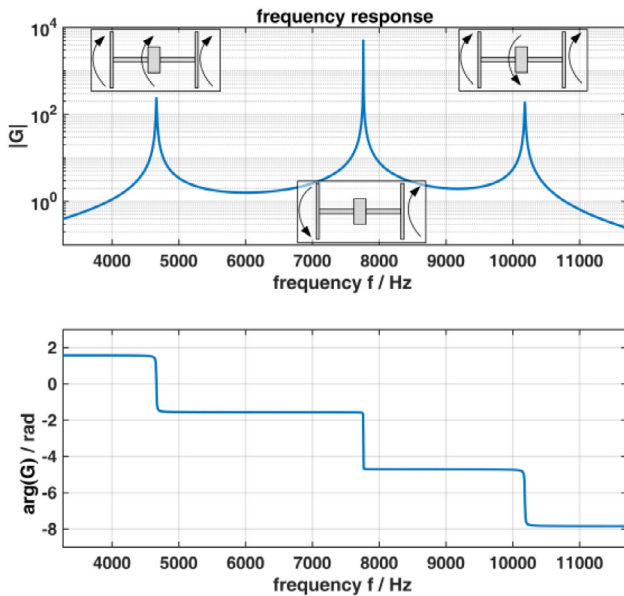
Figure 2. Sketch for 1D model.

Figure 3. Resonance behavior of the 1D model.

readout electronics a MFA200 module from Microresonant (a spin-off company of our institute)[3] is used. The module is based on hardware and algorithms presented in [15, 16].

Simulation

To devise the first design, a 1D model was used (see figure 2) consisting of three flywheels (moments of inertia J_1, J_2 and J_3), two torsional springs representing the outer pipe (spring constants: c_1 and c_2), and a torsional spring modeling the mounting structure (spring constant c_3). The deflection angles of the three flywheels are defined as φ_1, φ_2 and φ_3.

The differential equations for this model are simple and easy to handle. The actuation input for the system is a torque M_1 at the left side of the sensor (provided by the coils and permanent magnets). The output is the induced voltage at the right side, which is set proportional to $\dot{\varphi}_2 = \omega_2$. The linear time invariant (LTI) system can be described with a simple state space model. Figure 3 shows the transfer function between the input M_1 to the output $\dot{\varphi}_2$ of the model in frequency domain.

The three clearly visible resonances correspond to the symmetric, anti-symmetric and the higher order mode pointed out in figure 4. This simple model was used to design the
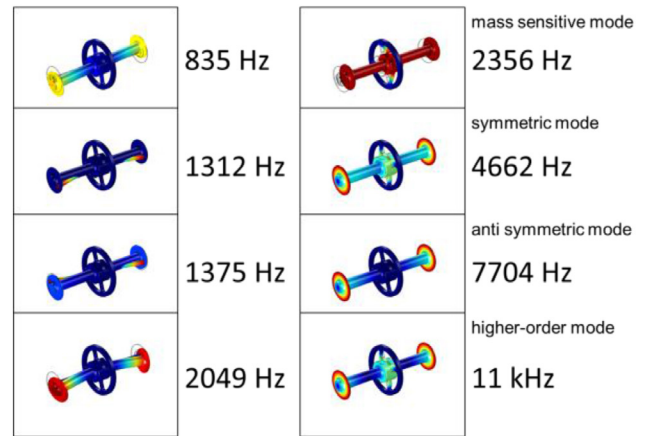
[3] www.micro-resonant.at

Figure 4. Different modes of the setup simulated in COMSOL. High deflection amplitudes are shown in red, lower deflection amplitudes in blue.

dimensions of the setup in order to achieve resonances that are easy to distinguish in terms of frequency. The most important design parameters are the moment of inertia of the flywheels J_1 and J_2, the spring constant of the outer pipes c_1 and c_2 and the fluid damping d_1 and d_2. The spring constants c_1 and c_2 can be calculated using a linear beam model. For the damping constants d_1 and d_2 a more accurate model is needed, the modeling of which is outlined in the next section.

After fixing the dimensions, a more complex COMSOL model was established to evaluate the frequencies of other modes not covered by the simple model.

Figure 4 shows the first eight modes of the mechanical resonator structure, where increasing deflection amplitude are color-coded from blue to red. The outer surface of the mounting spring was set as a fixed constraint. The relevant modes of the oscillator setup are shown on the right side in figure 4. The mode at 2356 Hz is mainly sensitive to the mass of the liquid. Here, both pipes and the contained liquid are moving along the longitudinal axis, i.e. they are oscillating against the mounting spring (see also [14]). Due to the mass of the liquid, the resonance frequency is shifted. The symmetric mode is at 4662 Hz. In this mode, both pipes are rotationally oscillating against the mounting spring. This mode has a larger sensitive surface because the wall speed is, in contrast to the anti-symmetric mode, approximately uniform along the length of the pipe. In this mode, the surface of the inner pipe is also moving and therefore interacting with the liquid. The mode is sensitive to the viscosity and the density of the liquid. This mode does not feature a node at the center, and therefore mechanical energy is coupled out via the mounting spring. As already noted, the most interesting mode of the setup is the anti-symmetric mode. This mode has its nodal point in the area where the pipe system is clamped to the mounting spring, reducing mechanical energy transfer to the housing. In this mode, the outer pipe acts as torsional springs between the two flywheels at its ends. As described above, the inner surface of the outer pipe interacts with the fluid. The sensitivity is higher at the ends of the pipe where the surface velocity peaks. The last oscillation mode shown is at 11 kHz and represents a higher order mode, where the
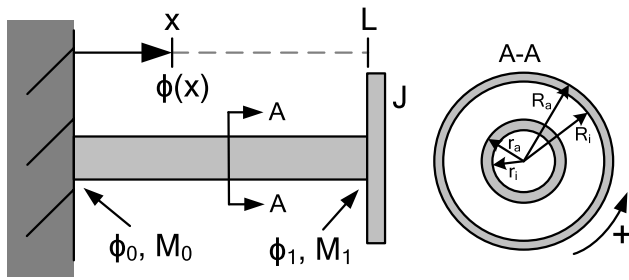
Figure 5. Reduced mechanical model for the anti-symmetric mode.

flywheels oscillate symmetrically against the mounting base in the center. This mode is also a torsional mode. In contrast to the anti-symmetric mode, this mode has two nodal points on the longitudinal axis which are not located at the mounting point of the pipe system, and therefore this mode has no advantage compared to the anti-symmetric mode. In this paper, we will mainly focus on the utilization of the anti-symmetric mode.

Fluid modeling

In order to incorporate the interaction with the fluid, a more accurate model for the mechanical oscillation was needed. To do so, the differential equation of a torsionally oscillating pipe featuring an inner pipe, which is considered to rest, was solved.

Figure 5 shows the considered geometry. First of all, a mechanical model for the empty resonator is derived. As the oscillation is anti-symmetric and the mounting spring is in the nodal point of the oscillator, it is sufficient to model only one half of the oscillator and to place a rigid wall at the center position. The 1D wave equation describing the transient problem is transformed to the frequency domain yielding a Helmholtz equation with complex torsional angle amplitudes ϕ and wavenumber k:

$$\frac{d^2}{dx^2}\phi = -k^2\phi, \tag{1a}$$

$$k = \frac{\omega}{\upsilon_T}, \tag{1b}$$

$$\upsilon_T = \sqrt{\frac{G}{\rho}}, \tag{1c}$$

where ω, υ_T, G and ρ denote angular frequency, bulk shear velocity, shear modulus and material density of the pipe, respectively. For the moment, the fluid loading is not considered, but is implemented in a later step by modifying the wavenumber k to a complex value.

The general solution to (1a) with expansion coefficients A and B is given by (2) and the boundary conditions are governed by (3) and (4):

$$\phi = A\cos(kx) + B\sin(kx), \tag{2}$$

$$\phi_0 = \phi(0), \ \phi_1 = \phi(L), \tag{3}$$

$$M_0 = M(0), \ M_1 = M(L), \tag{4}$$

where L denotes the length of the pipe. These general boundary conditions are chosen to allow for a representation using a transmission matrix relating torsional amplitudes and torques at $x = 0$ and $x = L$.

The relationship between the torque M and the contortion angle ϕ as well as the definition of the torsional moment of area I_T are given by

$$M = GI_T\frac{d}{dx}\phi,$$

$$I_T = \frac{\pi}{2}\left(R_a^4 - R_i^4\right),$$

where R_a and R_i are the outer and the inner radius of the outer pipe, respectively. The transmission matrix relating moment and angle can be derived using (2)–(4). For the rigid flywheels with a moment of inertia J connected at the end, the relation can be written as

$$\begin{bmatrix} \phi_0 \\ M_0 \end{bmatrix} = \begin{bmatrix} \cos(kL) & -\frac{\sin(kL)}{GI_Tk} \\ GI_Tk\sin(kL) & \cos(kL) \end{bmatrix} \begin{bmatrix} 1 \\ J\omega^2 \end{bmatrix} \phi_1.$$

The condition for the anti-symmetric mode is that $\phi_1 \neq 0$ exists for $\phi_0 = 0$, which leads to the transcendental equation

$$\cot(kL) = \frac{J\omega^2}{GI_Tk} \tag{5}$$

and can be transformed into a dimensionless form using (equations (1a)–(1c)) and introducing dimensionless frequency ε_n and system parameter a:

$$\varepsilon_n = a\cot(\varepsilon_n a).$$

The dimensionless frequency ε_n of vibrational mode n is defined by

$$\varepsilon_n = \frac{\omega_{r,n}}{\omega_0}, \ \omega_0 = \sqrt{\frac{GI_T}{JL}},$$

where ω_0 denotes the eigenfrequency of a system with a hypothetically massless torsion pipe. The dimensionless system parameter a is defined as

$$a = \omega_0\tau, \tau = L/\upsilon_T,$$

where τ is the propagation time of torsional waves along the length L of the pipe.

The intrinsic damping of the system can be taken into account by introducing a complex shear modulus $G^* = (G' + jG'')$, where $j = \sqrt{-1}$; the complex part of G^* models the damping.

Next the influence of the fluid is implemented in the model by calculating the drag forces at the inside of the outer pipe. For this, the model for an in-plane oscillating plate was used for the curved surface of the pipe. This is a valid approach when R_i is much larger than the penetration depth of the shear waves (see (6c)). The drag-force on an oscillating plate, placed parallel to a rigid wall at a distance H, can be calculated to (see also [17, 18])
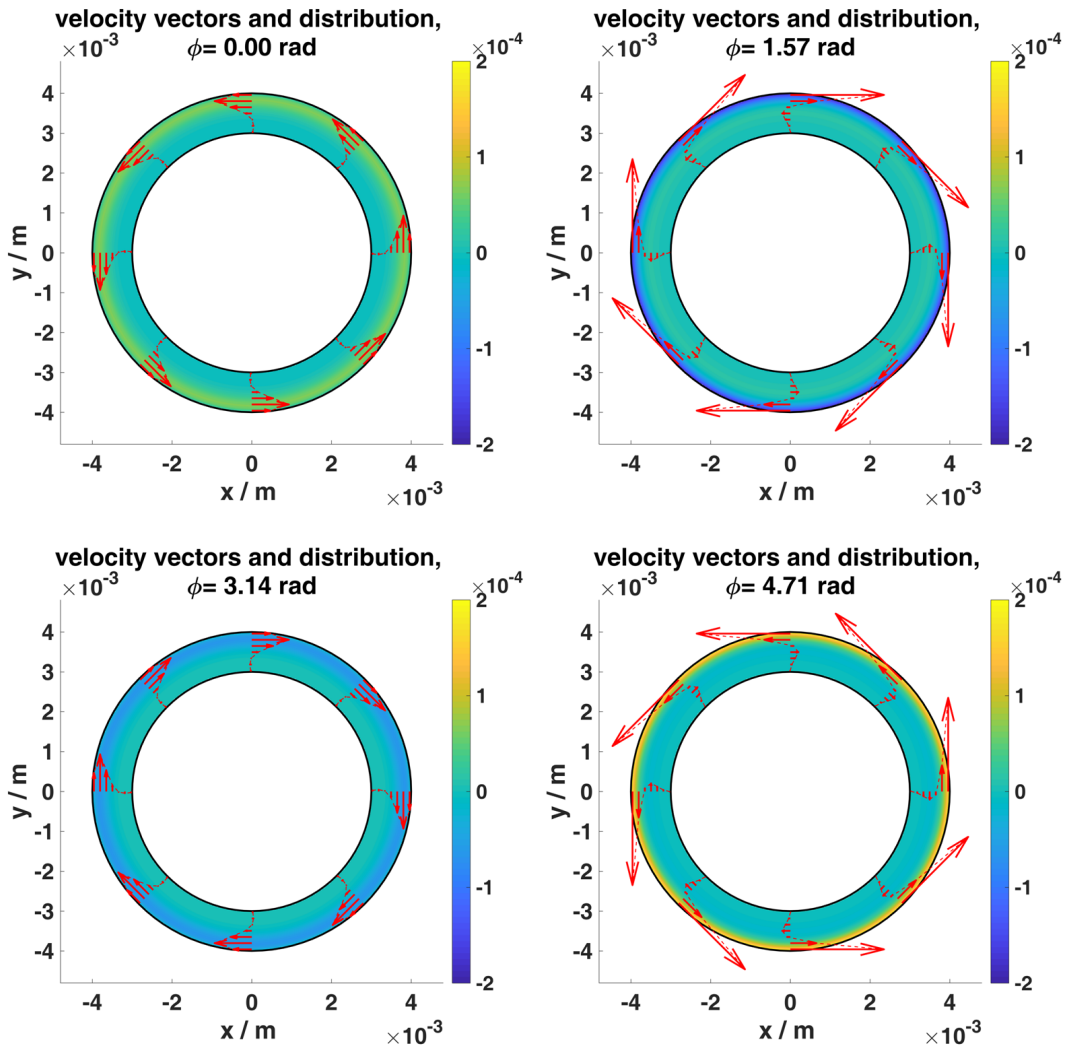
Figure 6. Shear wave and velocity distribution of a fluid in the sensor setup ($\rho = 1000 \, \text{kg m}^{-3}$, $\eta = 1$ Pa.s, $\omega = 48\,380 \, \text{rad s}^{-1}$, $\delta = 0.2 \, \text{mm}$). (Note: The viscosity was chosen high to improve the visibility of the shear wave.)

$$F_{\text{ps}} = -u_0 A \left(1 - j\right) \sqrt{\frac{\rho_{\text{f}} \eta_{\text{f}} \omega^3}{2}} K, \tag{6a}$$

$$K = \coth\left((1+j)\frac{H}{\delta}\right), \tag{6b}$$

$$\delta = \sqrt{\frac{2\eta_{\text{f}}}{\rho_{\text{f}} \omega}}, \tag{6c}$$

where u_0, A, ρ_{f}, η_{f}, ω and δ denote displacement, area, fluid density, fluid viscosity, angular oscillation frequency and penetration depth, respectively. The factor K accounts for the influence of the adjacent wall. K approaches unity when the penetration depth δ is small compared to the gap H such that the fluid space appears as an infinite half space.

Figure 6 shows the characteristic shear wave for an oscillating pipe for different times. In order to introduce this drag force into the model, we calculate the drag torque per length from (6a) (see also [17]):

$$\frac{\text{d}}{\text{d}x} M_{\text{ps}} = -\left(\pi R_i^3 \left(1 - j\right) \sqrt{2\rho_{\text{f}} \eta_{\text{f}} \omega^3}\right) K \phi\left(x\right). \tag{7}$$

In this equation the gap distance H in equation (6a) can be written as $R_{\text{i}} - r_{\text{a}}$, i.e. the difference of the inner radius of the outer pipe and the outer radius of the inner pipe. By inserting (7) into the differential equation of a damped torsional beam (see [19]) with an additional distributed damping torque M_{ps}:

$$GI_{\text{T}} \frac{\text{d}^2}{\text{d}x^2} \phi\left(x\right) + \omega^2 \rho I_{\text{T}} \phi\left(x\right) = -\frac{\text{d}}{\text{d}x} M_{\text{ps}}\left(x\right),$$

and bringing it to the following form:

$$\frac{\text{d}^2}{\text{d}x^2} \phi\left(x\right) = -k^2 \underbrace{\left(1 + 2\left(1 - j\right) \frac{\delta}{R_i} \frac{\rho_{\text{f}}}{\rho} \frac{K}{\frac{R_a^4}{R_i^4} - 1}\right)}_{\alpha(\omega)} \phi\left(x\right), \tag{8}$$

similar to equation (1a) with a complex-valued dimensionless correction term $\alpha(\omega)$. It is clearly visible that the sensitivity of the sensor can be influenced by the choice of R_{a} and R_{i}.
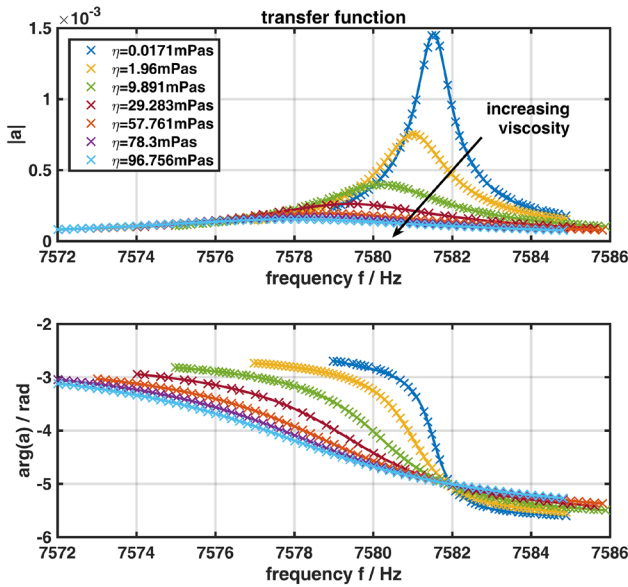
Figure 7. Resonance curve for different viscous fluids. With increasing viscosity the quality factor Q decreases and the resonance frequency f_r is shifted towards lower frequencies.

$$\varepsilon_n = \sqrt{\alpha}a \cot\left(\varepsilon_n\sqrt{\alpha}a\right). \qquad (9)$$

The complex dimensionless frequencies ε_n are determined numerically from equation (9) and the natural frequency and Q factor of the nth mode can be calculated by [20]

$$\omega_n = \mathrm{Re}\left\{\varepsilon_n\right\}\omega_0,$$

$$Q_n = \frac{\mathrm{Re}\left\{\varepsilon_n\right\}}{2\left|\mathrm{Im}\left\{\varepsilon_n\right\}\right|}.$$
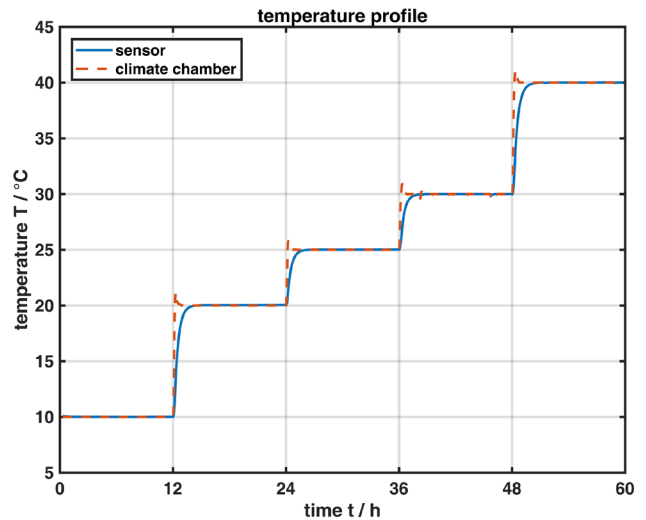
Measurements

The first measurements that were made were the resonance characteristics of the sensor setup for different viscosities. For this we used different water–glycerol mixtures. As readout electronics a MFA200 from Microresonant was used. Figure 7 shows the measured frequency response for different viscous liquids at 25 °C. The reference values were measured with a Stabinger™ Viscometer from Anton Paar. The air-filled sensor setup shows a very high quality factor Q of 9200. The damping in this case is caused mainly by the intrinsic losses of the material itself and the eddy current damping associated with the moving permanent magnets. The quality factor Q and the resonance frequency f_r were calculated using a frequency estimator [15].

The blue curve in figure 8 was fitted to the measurement results. This curve can be used as a calibration curve to calculate the viscosity.

To evaluate the temperature dependence and the accuracy of the resonator system, we measured 0W30 engine oil at different temperatures. The temperature influence on the sensor setup itself was modeled by equation (10), described in the next section.
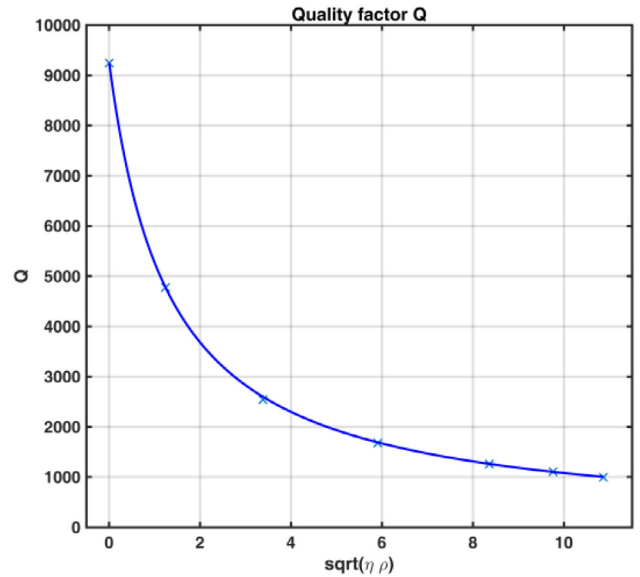

Figure 8. Fitting results for the quality factor Q of the measurements for the anti-symmetric mode.

Figure 9. Long-term measurements for five different temperatures. The red line shows the temperature measured by the climate chamber. The blue line is the temperature of the sensor system, provided by a PT100 mounted directly in the sensor system (see also figure 1(9)).

For the temperature measurements, the sensor setup was placed in a Weiss WKL 100 climate chamber. Due to the large thermal mass of the sensor system, a long settling time of 12 h was chosen. Figure 9 shows the temperature profile used for the measurements.

Figure 10 shows the response of the sensor setup during the whole measurement time. The quality factor Q increases with increasing temperature due to the decreasing viscosity of the fluid. The temperature steps are clearly visible. The quality factor Q changes from 914 to 1611 for viscosities η from 176 mPa · s to 42.3 mPa · s. (Note: The reference values for the viscosity and density were measured with a Stabinger™ Viscometer from Anton Paar, see table 1.) The resonance
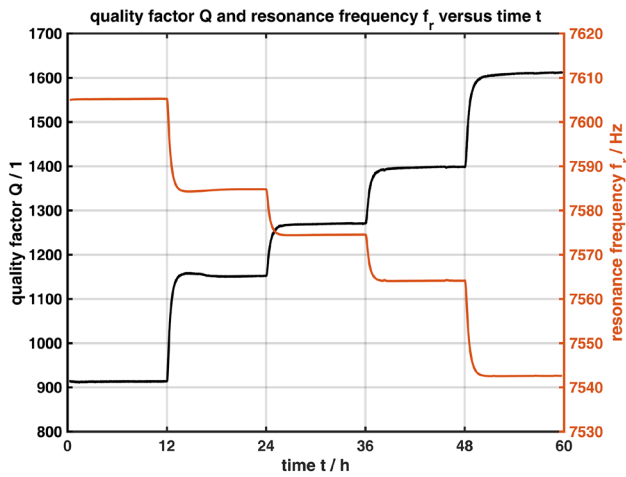
Figure 10. Quality factor Q and resonance frequency f_r of the sensor over time. The temperature was following the temperature profile shown in figure 9.

Table 1. Measured parameters for oil samples at different temperatures. The viscosity and density values were measured with a Stabinger™ Viscometer SVM 3000 from Anton Paar, the quality factor Q and the resonance frequency f_r were measured with a MFA200 from Microresonant.

| $T/°C$	$\eta/\text{mPa}\cdot\text{s}$	$\rho/\text{kg m}^{-3}$	$Q/1$	$\sigma(Q)$	f_r/Hz	$\sigma(f_r)$
10	176.01	837.3	913.5	0.27	7605.2	7.3×10^{-3}
20	102.86	831.0	1151.8	0.35	7584.8	4.3×10^{-3}
25	80.643	827.9	1270.3	0.35	7574.5	7.7×10^{-3}
30	64.165	824.7	1398.6	0.31	7564.1	30.7×10^{-3}
40	42.306	818.5	1611.4	0.38	7542.6	14.8×10^{-3}

frequency, on the other hand, decreased from 7605 Hz to 7542 Hz.

Figure 11 shows a histogram of the quality factors Q which were determined at different sampling times. The lower plot illustrates the measurement spread for a particular temperature (25 °C in this example). For each temperature step, only samples during the final 2 h were used to account for the temperature settling of the setup. This measurement series demonstrates the temperature dependency of the oil's viscosity.

Table 1 shows the measured parameters. The reference values for viscosity and density were measured using the aforementioned Stabinger™ Viscometer SVM 3000 from Anton Paar. The value for the quality factor Q and the resonance frequency f_r are the mean values of the last 757 values (sampled during approx. 2 h) for each temperature step; the σ value is the associated standard deviation.

Discussion

In order to calculate the viscosity from the measured parameters, a simplified model is introduced, preserving the structure of the model previously developed (see equation (7)). As for the measured viscosity range, the penetration depth $\delta = \sqrt{\frac{2\eta}{\rho\omega}}$
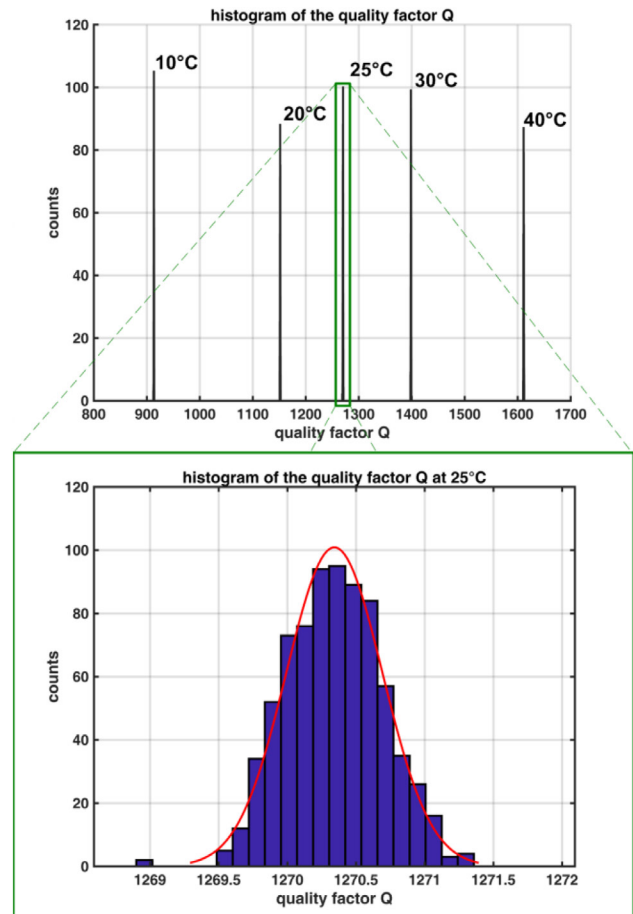
Figure 11. Histogram of the quality factor Q measurements, of the last 2 h for each temperature shown in figure 10.
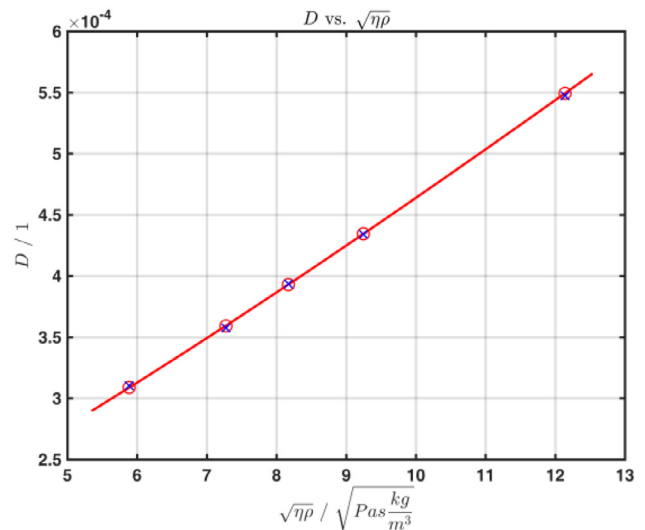
Figure 12. Damping factor $D = 1/(2Q)$ versus $\sqrt{(\eta\rho)}$.

of the shear displacement wave is small compared to the distance H; the factor K in equation (6a) can be neglected. We end up with a simplified model for the quality factor Q (see also [21]):
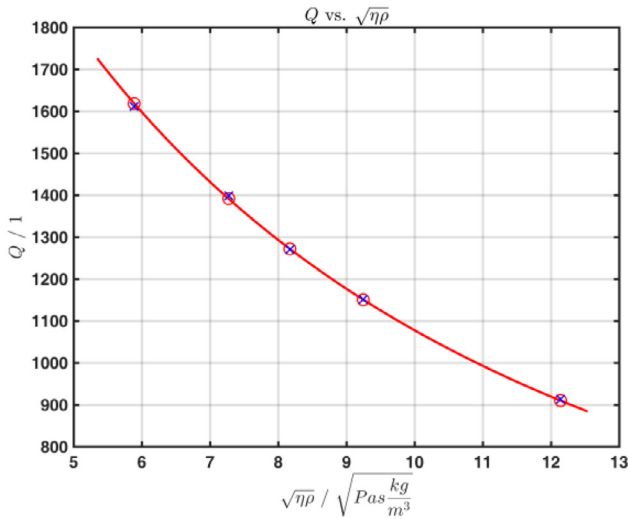
Figure 13. Quality factor Q versus $\sqrt{(\eta\,\rho)}$.

Table 2. Calculated viscosity.

T/°C	η/mPa · s	ρ/kg m^{-3}	η_{calc}/ mPa · s	Relative $\sigma(\eta_{\mathrm{calc}})$ %	Relative error %
10	176.01	837.3	174.67	0.063	0.762
20	102.86	831.0	102.64	0.068	0.217
25	80.643	827.9	80.09	0.064	0.326
30	64.165	824.7	63.44	0.053	1.129
40	42.306	818.5	42.77	0.064	1.105

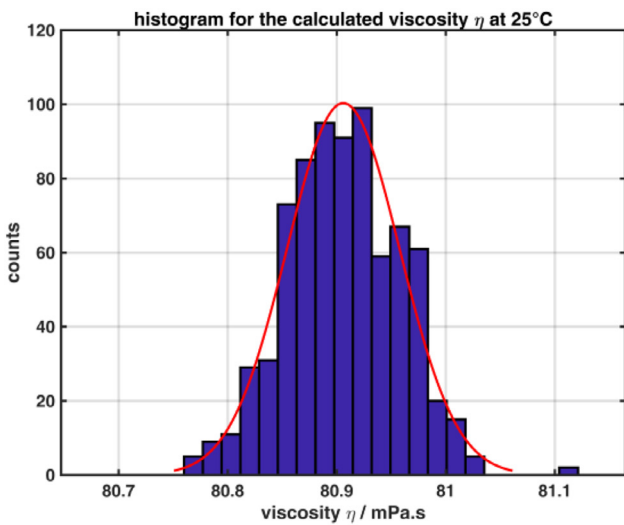**Figure 14.** Histogram of the viscosity η determined from the measured quality factor Q, temperature T, resonance frequency f_{r} and density ρ (compare figure 11).

$$D = \omega\left(x_1\sqrt{\eta\rho\omega} + x_2 T + x_3\right), \qquad (10)$$

$$Q = \frac{1}{2D}, \qquad (11)$$

where x_1, x_2 and x_3 are fitting parameters depending on the geometry, the temperature dependency and the intrinsic damping of the setup. In this empirical model a linear temperature dependence of the intrinsic damping was assumed. As the relative change in temperature is relatively small (a range of 30 °C was covered), this assumption was considered justified for a first-order approximation.

Figures 12 and 13 show that the simplified model derived from equation (10) matches well with the measurements. To calculate the viscosity from the measured parameters, equations (10) and (11) are solved for η. (Note: To do so the density of the fluid has to be known from additional measurements, in our case we used the values obtained with the Stabinger™ Viscometer.)

The relative errors for the calculated viscosities η_{calc} are very low (see table 2): all relative errors are smaller than 1.13%. For this estimation the mean values of the measurement points used in figure 14 were compared to the reference values measured with the Stabinger™ Viscometer.

The standard deviation is small compared to the relative error of the viscosity measurement, which means that the relative error can be reduced by refining the model and improving the temperature control of the setup.

Conclusions

We presented a viscosity measurement setup based on a balanced torsionally resonating pipe with two flywheels and electromagnetic actuation and readout. We performed measurements at five different temperatures to evaluate the accuracy and the stability of the measurement system. We developed different accurate models for the design as well as for the calibration of the model. Measurements with a Stabinger™ Viscometer were used to calibrate the temperature-dependent model derived in equation (10). Doing so, a high accuracy with a relative error smaller than 1.13% for viscosity η (see table 2) could be achieved.

In a next step we will increase the viscosity range to much higher values so that the influence of the inner pipe is also visible. In so doing, the penetration depth of the shear wave (equation (6c)) could be increased and the influence of the inner pipe will no longer be negligible anymore. The parameter K (equation (6b)) will differ from one and the simplified model in equation (10) will not be valid anymore.

Acknowledgments

ORCID iDs

S Clara https://orcid.org/0000-0002-2668-5146
B Jakoby https://orcid.org/0000-0002-2918-7150

References

[1] Biechele P, Busse C, Solle D, Scheper T and Reardon K 2015 Sensor systems for bioprocess monitoring *Eng. Life Sci.* **15** 469–88

[2] Kroll P, Sagmeister P, Reichelt W, Neutsch L, Klein T and Herwig C 2014 *Ex situ* online monitoring: application, challenges and opportunities for biopharmaceuticals processes *Pharm. Bioprocess.* **2** 285–300

[3] Macosko C W 1994 *Rheology, Principles, Measurements and Applications* (New York: Wiley) ISBN: 978-0-471-18575-8

[4] Kroger D 2002 Stabinger Viscometer *Petro Industry News* vol 3 issue 4 Annual Buyers Guide 2002/2003

[5] Jakoby B, Beigelbeck R, Keplinger F, Lucklum F, Niedermayer A, Reichel E K, Riesch C, Voglhuber-Brunnmaier T and Weiss B 2010 Miniaturized sensors for the viscosity and density of liquids-performance and issues *IEEE Trans. Ultrason. Ferroelectr. Freq. Control* **57** 111–20

[6] Heinisch M, Reichel E K, Dufour I and Jakoby B 2014 A U-shaped wire for viscosity and mass density sensing *Sens. Actuators* A **214** 245–51

[7] Martin S J, Granstaff V E and Frye G C 1991 Characterization of a quartz crystal microbalance with simultaneous mass and liquid loading *Anal. Chem.* **63** 2272–81

[8] Reichel E K, Riesch C, Keplinger F, Kirschhock C E A and Jakoby B 2010 Analysis and experimental verification of a metallic suspended plate resonator for viscosity sensing *Sens. Actuators* A **162** 418–24

[9] Martin S J, Cernosek R W and Spates J J 1995 Sensing liquid properties with shearmode resonator sensors *Transducers, Eurosensors IX* pp 712–5

[10] Heinisch M, Voglhuber-Brunnmaier T, Reichel E K, Dufour I and Jakoby B 2015 Application of resonant steel tuning forks with circular and rectangular cross sections for precise mass density and viscosity measurements *Sens. Actuators* A **226** 163–74

[11] Abdallah A, Reichel E K, Voglhuber-Brunmaier T, Heinisch M, Clara S and Jakoby B 2015 Symmetric mechanical plate resonators for fluid sensing *Sens. Actuators* A **232** 319–28

[12] Rahafrooz A and Pourkamali S 2011 Characterization of rotational mode disk resonator quality factors in liquid *Proc. 2011 Joint Conf. of the IEEE Int. Frequency Control and the European Frequency and Time Forum (FCS) (San Francisco, CA)* pp 1–5

[13] Jakoby B and Vellekoop M J 2004 Physical sensors for water-in-oil emulsions *Sens. Actuators* A **110** 28–32

[14] Clara S, Antlinger H, Feichtinger F, Niedermayer A O, Voglhuber-Brunnmaier T and Jakoby B 2017 A balanced flow-through viscosity sensor based on a torsionally resonating pipe *IEEE Sensors (Glasgow)* (https://doi.org/10.1109/ICSENS.2017.8234137)

[15] Niedermayer A O, Voglhuber-Brunnmaier T, Sell J and Jakoby B 2012 Methods for the robust measurement of the resonant frequency and quality factor of signifcantly damped resonating devices *Meas. Sci. Technol.* **23** 085107

[16] Niedermayer A O, Voglhuber-Brunnmaier T, Heinisch M, Feichtinger F and Jakoby B 2016 Monitoring of the dilution of motor oil with diesel using an advanced resonant sensor system *Procedia Eng.* **168** 15–18

[17] Heinisch M, Voglhuber-Brunnmaier T, Reichel E K, Dufour I and Jakoby B 2015 Electromagnetically driven torsional resonators for viscosity and mass density sensing applications *Sens. Actuators* A **229** 182–91

[18] Landau L D and Lifshitz E M 1987 *Fluid Mechanics* (Portsmouth, NH: Heinemann) ISBN: 978-0080339337

[19] Graft K F 1991 *Wave Motion in Elastic Solids* (New York: Dover) ISBN: 978-0486667454

[20] Auld B A 1990 *Acoustic Fields and Waves in Solids* (Malabar, FL: Krieger Pub Co) ISBN: 978-0898747829

[21] Heinisch M, Voglhuber-Brunnmaier T, Reichel E K, Dufour I and Jakoby B 2014 Reduced order models for resonant viscosity and mass density sensors *Sens. Actuators* A **220** 76–84